ISA Transactions 131 (2022) 650–661

Contents lists available at ScienceDirect

ISA Transactions

journal homepage: www.elsevier.com/locate/isatrans

Practice article

An optimization method for motion blur image restoration and ringing suppression via texture mapping

Wensheng Wang [a,b], Chang Su [c,*]

[a] School of Mechanical and Electrical Engineering, Beijing Information Science and Technology University, Beijing, China
[b] Key Laboratory of Modern Measurement and Control Technology, Ministry of Education, Beijing Information Science and Technology University, Beijing, China
[c] Changchun Institute of Optics, Fine Mechanics and Physics, Chinese Academy of Sciences, Changchun, China

ARTICLE INFO

Article history:
Received 22 July 2021
Received in revised form 4 May 2022
Accepted 4 May 2022
Available online 13 May 2022

Keywords:
Image sensor
Image deconvolution
Richardson–Lucy algorithm
Ringing-detecting regularization
Texture map
Adaptive optimization iteration

ABSTRACT

Since the image sensor will produce blur problems in the process of collecting data of moving objects, the image needs to be restored. Ringing is one of the most common artifacts in deblurred images. This paper proposes a non-blind image deconvolution method based on texture mapping segmentation, named texture-Richardson–Lucy (TRL) algorithm, which suppresses ringing while deblurring the image. TRL is based on a novel ringing removal deconvolution algorithm, which adds a ringing detection term as regularization in the iterative process of the Richardson–Lucy algorithm. Taking into account the structural difference between the texture and the flat area, the image is segmented into several blocks and restored through adaptive iterative texture maps based on the pixel intensity and texture features of the image. In order to obtain a reasonable texture map, a Gaussian mixture model is used to fit the pixel intensity distribution, and use the expectation maximization algorithm and local binary mode to estimate. Experimental results and quantitative evaluations show that TRL can effectively reduce ringing artifacts while retaining details and achieving robustness to suppress ringing of different blur kernels. The processing time of a single 1 million pixel image in an 8-core CPU environment is about 3.5 s. And the PSNR and SSIM parameters are above 30 dB and 0.92, respectively. In conclusion, TRL is superior to the current popular algorithms.

1. Introduction

Image blur can be caused by factors such as focal length, camera shake, and movement of target objects. Image motion blur is an image degradation phenomenon caused by the relative displacement between the subject and the camera in an exposure. The relative displacement will cause pixels in different positions to overlap, resulting in reduced imaging quality. As one of the most common image degradation phenomena, motion blur exists widely in many visual processing tasks. In different image application fields, such as astronomy, military, medicine, industrial control, road monitoring and criminal investigation, high-quality clear images are important in collecting image information for various analysis. Therefore, the problem of motion blurred image restoration has always been the focus of research worldwide.

One of the most obstinate problems in photography is blurring caused by various blur sources, such as atmospheric turbulence, an out-of-focus lens and relative motion between the camera and the scene. These blur sources can be modeled as a blur kernel K, convolved with the true image intensities L, which will generate the degraded image B, as follows:

$$B = L \otimes K + N \tag{1}$$

where $\otimes$ denotes the discrete image convolution and N is an additive noise term. Removing that blur from captured image B is thus a form of image deconvolution, which is an ill-posed inverse problem with a long history in many scientific applications.

To address this issue, deconvolution approaches, such as the Wiener filter [1], the regularized filter [2], the Richardson–Lucy (RL) algorithm [3,4], the total variation deconvolution [5–7], and deconvolution by a Sparse Prior [8], have been proposed. However, the deblurred image usually contains a number of artifacts because the blur often introduces zeros in the frequency domain with high frequencies truncated and information lost. In addition, it is challenging to estimate a blur kernel accurately in the presence of unavoidable noise because of the use of photo-sensors and signal transmission. Manchester [9] proposed the existence of Koopman eigenfunctions for a class of nonlinear models using Koopman learning theory. This cutting-edge achievement is considered to be applied to the field of image restoration as our next research direction.

* Corresponding author.
E-mail address: suchang906@163.com (C. Su).

https://doi.org/10.1016/j.isatra.2022.05.005
0019-0578/

Null frequencies in the blur kernel, an inaccurate kernel, and the presence of noise are common causes of excessively amplified noise and ringing artifacts, the two most universal consequent artifacts in deblurred images. Ringing artifacts are periodic light and dark ripples around the edge and may span across an image. They are extremely difficult to eliminate after the deconvolution because they are mixed with the image structures at the mid-frequency band. In addition, large-scale ringing artifacts cause substantially more harm to the quality of the deconvoluted image than do noise and blur [10].

Depending on whether the blur kernel is known, image deconvolution is usually separated into the non-blind and blind cases. In this paper, a non-blind deconvolution is concentrated on where the kernel is acquired by relational methods, and only the latent sharp image needs to be restored from the observed blurry image. Many methods have been developed to estimate or determine the kernel, for instance, from an accelerometer and/or a gyroscope [11], a secondary sensor [12], a known synthetic pattern [13], a single image [14–16].

An improved Richardson–Lucy algorithm named texture-Richardson–Lucy (TRL) algorithm is proposed. It restores images with explicitly fewer ringing artifacts and well-maintained details. Two pivotal improvements are proposed based on RL algorithm. First, TRL uses a multiscale image pyramid to measure ringing artifacts and a regularization term to suppress them. Second, image pixels are classified by a Gaussian mixture model. Pixels with the same Gaussian distribution are divided into the same class, forming a unique texture map. Every class is iterated a diverse number of times based on its flatness and similarity texture feature, achieving a better reconstruction effect of the image and suppressing the ringing between different areas. This approach has a significant effect on regenerating sharp edges and details and constraining the ringing artifacts.

The remainder of the paper is structured as follows: In Section 2, the related work and the differences in our approach are reviewed. In Section 3, an adaptive regularization algorithm is introduced to eliminate ringing by adding a ringing-detecting term in the minimization and iterating adaptively via a texture map. The ringing artifact removal and segmentation-based iteration scheme are presented. In Section 4, the results of TRL for real blurry images are presented; conclusions follow in Section 5.

2. Related work

Removing ringing is one of the most challenging problems in image deconvolution. There have been several methods that provide superior performance for this problem in the literature in the past decades. Additional details concerning classic methods can be found in [17]. This paper is primarily focused on the work relevant to our approach.

One of the most common non-blind image deconvolution approaches is the RL algorithm [3,4], which is an iterative algorithm that takes image intensities as Poisson statistics to transform the inverse problem into exploring a maximum likelihood solution. This approach can be used effectively in many deblurring processes, but its results still contain noticeable ringing artifacts. In addition, this method applies the same operation to both smooth and textured regions during the iterative process, which intensifies ringing artifacts parallel to image edges as the number of iterations increases.

The ringing, one of the troubling artifacts at image edges or boundaries in the deconvolution stage, was also addressed in abundant literature. Whyte et al. [18] analyzed causes of ringing artifacts in general and proposed a deblurring algorithm in order to reduce ringing, which located these bright pixels in the latent sharp image and separate them from the remainder of the latent image. They pointed out that ringing can only be suppressed, but not eliminated in image restoration. Shan et al. [15] introduced a model of the spatial randomness of noise in the blurred image and a local smoothness prior to reducing ringing artifacts, which constrains contrast in the unblurred image wherever the blurred image exhibits low contrast. Image edges can be kept by introducing a segmentation-based regularization term. However, using smoothing to suppress ringing can lead to a new blur in the restored image. Cho et al. [19] regarded saturation pixels and non-Gaussian noise as outliers and built a non-blind deconvolution method in a blur model that considers these outliers to reduce the visual artifacts they cause. The visual artifact area is located and removed through outliers. The artifact area is required to be accurately recognized, requiring high accuracy of the algorithm. Yang et al. [20] modeled the latent variable as a set of independent random variables and regularized these variables by the prior motivated from edge selection/reweighting. In addition, Pan et al. [21] proposed an ℓ_0-regularized prior based on the distinctive properties of text images and selected salient edges as stronger piecewise priors for text image deblurring. This algorithm can recover natural images with complex scenes and low illumination. The authors used the edge method to suppress the ringing, which inspired us to suppress the ringing according to the area. Ringing is mainly generated from the edge. The edge of the image is the transition zone between one low-frequency area and the other low-frequency area. If the different low-frequency regions in the image are found out and processed separately, there will be no ringing.

Due to the recent success of Convolutional Neural Networks (CNN) and Generative Adversarial Networks (GAN) in object detection [22], recognition [23] and related tasks [24], several CNN-based methods have been proposed for image deblurring [25]. We analyze the development of image restoration algorithms in the field of deep learning, and compare the processing results of deep learning image restoration algorithms in recent years. Zhang et al. [26] integrated model-based optimization methods with discriminative learning methods. They trained a set of CNN denoisers that were integrated into the model-based optimization method to solve inverse problems. Li and Pan [27] presented a blind image deblurring method based on a data-driven discriminative prior. And this image prior is treated as a binary classifier to distinguish whether an input image is clear or not and embedded it into the maximum a posterior to help blind deblurring. Shen et al. [28] presented a human-aware convolutional neural network which integrated foreground/background deblurring models with a supervised attention mechanism for global and harmonious deblurring. Lu et al. [29] proposed an unsupervised method to disentangle the content and blur features in a blurred image and added a blurring branch and cycle-consistency loss to remove unrealistic artifacts. Kaufman and Fattal [30] broke the deblurring network into an analysis network for estimating the kernel, and a synthesis network for deblurring the image. The above methods to generate different blur kernels are used to compare the effects of TRL algorithm under these blur kernels.

These approaches attempt to implicitly handle ringing artifacts by finding a better balance between ringing suppression and detail conservation in the recovered image. TRL shows that ringing artifacts can be more effectively eliminated by explicitly adaptively iterating the image with the regularized deconvolution algorithm. The potential of our model in general image restoration is demonstrated, and a subjective study on the deblurring quality of real blurred images is conducted. At the same time, three popular benchmarks (PSNR, SSIM, and efficiency) to demonstrate the most advanced performance achieved by TRL are used to compare popular algorithms. The quantitative indicators PSNR and SSIM are stable at around 30 dB and 0.94 respectively. In terms of efficiency, TRL is faster than these popular algorithms.

3. Texture-Richardson–Lucy (TRL) algorithm

Based on standard RL algorithms, a ringing-detecting term is added into this algorithm as a regularization to suppress ringing artifacts and preserve the edges in the deconvolution process. Built on this regularized algorithm, adaptive iterations are applied to the blurred image by its texture features to recover additional details in texture regions and to prevent flat regions from overestimating.

The RL algorithm assumes that the image noise submits to the Poisson distribution, and the likelihood probability of the image L can be denoted as:

$$p(B|L) = \prod_{x} \frac{(L \otimes K)^{B} \exp[-(L \otimes K)]}{B!} \tag{2}$$

Because the maximum likelihood solution of $p(B|L)$ is also the minimum solution of the corresponding $-\log[p(B|L)]$ function, maximizing the likelihood is equivalent to minimizing the energy function:

$$L^{*} = \arg\min_{L} E(L) \tag{3}$$

where

$$E(L) = \sum \left[(L \otimes K) - B \cdot \log(L \otimes K) \right] \tag{4}$$

Setting the derivative of $E(L)$ equal to zero with the kernel constraint $\sum_{x} K(x) = 1$, by the RL algorithm, the iterative estimation of the image can be generated as follow:

$$L^{r+1} = L^{r} \left[K^{*} \otimes \frac{B}{(L^{r} \otimes K)} \right] \tag{5}$$

where K^{*} is the adjoint of K and r is the iterative number. This algorithm not only preserves the total energy of images in the iteration process but also maintains the approximated values as nonnegative if the starting approximation is nonnegative. However, because its iterative number is uncertain, additional image details and ringing artifacts are simultaneously introduced as the number of iterations increases.

3.1. No-Reference ringing-detecting term as a regularization

To reduce ringing artifacts in deconvolution, the first consideration is to detect and quantify them in images. A method to measure large-scale ringing was proposed by Liu et al. [10], which estimates ringing in flat regions, but avoids image structures in textured regions. Similarly, one multiscale ringing-detecting term is adopted as a regularization term to the energy in Eq. (3):

$$L^{*} = \arg\min_{L} \left[E(L) + \lambda E_{R}(L) \right] \tag{6}$$

where λ is the regularization factor and the term $E_{R}(L)$ is defined as:

$$\begin{aligned} E_{R}(L) = \sum_{x=1}^{X} \frac{1}{2} \Big(& \| S_{h} \otimes G_{x-1} \otimes L^{r} - S_{h} \otimes G_{x} \otimes L^{r} \|_{2}^{2} \\ & + \| S_{v} \otimes G_{x-1} \otimes L^{r} - S_{v} \otimes G_{x} \otimes L^{r} \|_{2}^{2} \Big) \end{aligned} \tag{7}$$

where $\| \bullet \|_{2}$ denotes the ℓ_{2}-norm function, G_{x} is a scaled Gaussian blur kernel with the size of $4x + 1 (x = 0, 1, 2 \ldots X)$, and S_{h} and S_{v} denote the horizontal derivative operator and the vertical derivative operator, respectively. Here, the noise robust gradient operators that Holoborodko proposed are used. Combining isotropic noise suppression and precise partial derivatives estimation, the operators can effectively perceive horizontal and vertical high frequencies and avoid the details and the noise being detected [31]. The horizontal operator is presented as follows, and the vertical operator is simply a 90-degree rotation of the horizontal operator:

$$S_{h} = \frac{1}{32} \begin{bmatrix} -1 & -2 & 0 & 2 & 1 \\ -2 & -4 & 0 & 4 & 2 \\ -1 & -2 & 0 & 2 & 1 \end{bmatrix} \tag{8}$$

To obtain the solution of the updated formula, Eq. (6) is minimized, and then a regularized RL algorithm is obtained:

$$L^{r+1} = \frac{L^{r}}{1 + \lambda \nabla E_{R}(L^{r})} \left[K^{*} \otimes \frac{B}{(L^{r} \otimes K)} \right] \tag{9}$$

where

$$\begin{aligned} \nabla E_{R}(L) = \sum_{x=1}^{X} \Big(& S_{h}^{*} \otimes S_{h} \otimes (G_{x-1} \otimes L - G_{x} \otimes L) \\ & + S_{v}^{*} \otimes S_{v} \otimes (G_{x-1} \otimes L - G_{x} \otimes L) \Big) \end{aligned} \tag{10}$$

where S_{h}^{*} and S_{v}^{*} are adjoints of S_{h} and S_{v}, respectively.

From Eq. (9), the deviation of $E_{R}(L)$ places a penalty on ringing artifacts and regularizes each pixel. The $E_{R}(L)$ is based on the idea that the larger Gaussian blur kernel can make the images smoother, including wavy ringing; moreover, the differences between the edges of images blurred by G_{x-1} and G_{x} are mainly ringing artifacts. In addition, these differences are expected to have little distinctions in larger-sized blurs, while the differences are significant in smaller-sized blurs. Therefore, the sum of the multiple-level detection results should push the $E_{R}(L)$ towards ringing artifacts instead of real edges.

Image quality metrics commonly include PSNR [32] and multiscale SSIM [33]. PSNR (Peak Signal-to-Noise Ratio) is the most common and widely used image objective evaluation metric, which is based on the corresponding pixel point. It is based on the error-sensitive image quality evaluation. PSNR is often expressed in logarithmic decibel units. A larger value equals better image quality. However, human eyes are more sensitive to the contrast difference with lower spatial frequency and the contrast difference of brightness instead of chromaticity. Since the visual characteristics of human eyes are not considered, there will be inconsistencies between the evaluation results and human eyes' subjective perceptions. SSIM (structural similarity index measure) is a type of measurement of image similarity. From the perspective of image composition, structure information is defined as properties that reflect the structure of objects in the scene independently of brightness and contrast. Distortion is modeled as a combination of three different factors brightness, contrast, and structure. The mean is used as an estimate of brightness, the standard deviation is used as an estimate of contrast, and the covariance is used as a measure of structural similarity. Their values can better reflect the subjective feeling of the human eye.

Fig. 1 shows a comparison of standard RL and TRL algorithms. The motion blur image is generated by adding the motion blur of the known blur kernel to the original clear image, and both algorithms are iterated 50 times. In the ringing-detecting regularization term, three resolution levels are considered as default, i.e., $X = 3$. Although both the standard RL algorithm and the TRL algorithm with ringing-detecting regularization cannot recover all the details due to high frequency loss, the results still show that this regularized algorithm can generate images with fewer ringing artifacts and well-preserved image edges compared to the standard RL algorithm. Peak Signal-to-Noise Ratio (PSNR) and Structural Similarity (SSIM) are used to compare RL and TRL algorithms. The PSNR of TRL is 30.13 dB, which is 2.6 dB higher than that of RL; the SSIM of TRL is 0.912, which is 0.15 higher than that of RL.

(a) (b) (c) (d)

Fig. 1. Effect of the regularization in the proposed deblurring model. (a) Original Lena image. (b) Blurred Lena image with Gaussian blur. (c) Standard RL result. (d) The result of the improved RL with ringing-detecting regularization.

Algorithm 1 Deblurring algorithm with ringing-detecting regularization and segmentation-based texture map

Input: blurred image: B; blur kernel K; resolution level X; regularization factor λ; number of clusters Q; number of iterations t

Output: deblurred image L_{final}

procedure INITIAL DEBLURRED IMAGE
- $L^0 = B, r = 0$
- Update:

$$\nabla E_R(L^r) = \sum_{x=1}^{X}\Big(S_h^* \otimes S_h \otimes (G_{x-1} \otimes L^r - G_x \otimes L^r) + S_v^* \otimes S_v \otimes (G_{x-1} \otimes L - G_x \otimes L^r)\Big)$$

$$L^{r+1} = \frac{L^r}{1+\lambda \nabla E_R(L^r)}\left[K^* \otimes \frac{B}{(L^r \otimes K)}\right]$$

$r = r + 1$

until $r > 4$

end procedure

procedure GENERATE TEXTURE FEATURE MAP m
- Using EM approach to divide the image into Q sections;
- Calculate the LBP of each section;
- Rank sections according to LBP value of each section:

$Z = Q$

Do:

$m = \frac{Z}{Q}$ for the section which has the largest LBP value

delete the largest LBP value

$m = m - 1$

Until Z<1

end procedure

procedure FINAL DEBLURRED IMAGE L_{final} - $L^0 = L_{init}, r = 0$
- Update for each section:

$$\nabla E_R(L^r) = \sum_{x=1}^{X}\Big(S_h^* \otimes S_h \otimes (G_{x-1} \otimes L^r - G_x \otimes L^r) + S_v^* \otimes S_v \otimes (G_{x-1} \otimes L - G_x \otimes L^r)\Big)$$

$$L^{r+1} = \frac{L^r}{1+\lambda \nabla E_R(L^r)}\left[K^* \otimes \frac{B}{(L^r \otimes K)}\right]$$

$r = r + 1$

until $r > m * t$

Return: The deblurred image L_{final}

end procedure

3.2. Adaptive iterations by texture feature map

Because the ringing-detecting term inevitably misclassifies parts of image edges as ringing, the introduced regularization not only suppresses the ringing artifacts in the iterative process but tends to smooth the whole restored image, including regions with ample textures. One simple method for addressing this situation is to increase the number of iterations, but this will result in more artifacts in both textured and flat regions even if the regularized RL algorithm is used. Therefore, based on the regularized RL algorithm, we further apply different iterations to diverse regions to adequately restore details in textured regions and lessen the overestimates of the flat regions of the image.

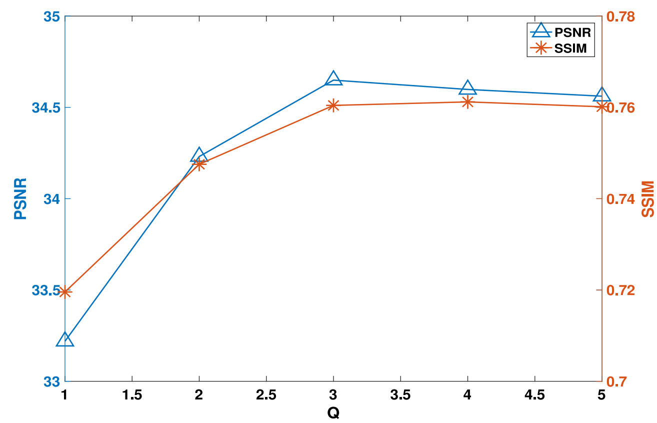

Fig. 2. Quantitative evaluations of recovered images with various Q.

A Gaussian mixture model is used where the classifications of the image are estimated by fitting Gaussian conditional pixel intensity distributions. The main idea of this method is to classify pixels into Q categories according to the fitting result and to rank the region whose pixel intensities belong to the same category in proportion to the complexity of its texture feature. For classification, a texture feature map m is generated. In matrix m, for the area with the roughest texture, the element of matrix m is set as value 1; and for the flattest area, the element of matrix m is set as value 1/Q. The values of other regions increase sequentially in steps of 1/Q. For each rank, a different number of iterations in the deconvolution process is adopted.

To know the map m, the maximum likelihood estimation of the Gaussian mixture model by the expectation maximization (EM) algorithm is first acquired. Then, the image is partitioned into Q sections and pixels in each section subject to the same Gaussian distribution with the same mean and variance. Finally, the local binary pattern (LBP) is used to assess the image textures. The sum of the normalized LBP of pixels of each section is calculated and used to rank these sections to obtain the texture feature map m.

Fig. 2 shows an example of deblurring results with various Q to illustrate the impact of the number of partitions on the quality of the restorations. The figure is divided 1(a) into Q categories, with the Q between [1, 5] and plots the variation of PSNR and

(a) (b)

Fig. 3. Deblurring the synthetically blurred image from Fig. 1(b). (a) The texture map of blurry Lena. (b) The result by TRL algorithm.

(a) (b) (c) (d)

Fig. 4. Effects of the λ with different values. (a) $\lambda = 0.1$. (b) $\lambda = 0.5$. (c) $\lambda = 0.7$. (d) $\lambda = 0.9$.

SSIM of restored images. In this example, when Q becomes larger than about three, PSNR and SSIM level off. That is, as the number of sections is increased, PSNR and SSIM are decreased since more areas are over-fitting to cause more ringing artifacts. Therefore, Q is set to three for all examples.

The texture feature map m and the result deblurred by TRL algorithm are shown in Fig. 3. For comparison, Fig. 1(b) remains as the blurred input. To obtain an accurate texture map, the fitting of the Gaussian mixture model and ranking by texture feature are conducted after five iterations for all examples. Compared with the results in Figs. 1(c) and 1(d), the quality of the recovered image in Fig. 3(b), which comprises less ringing and more detail, is further improved by this segmentation-based scheme.

As shown in Fig. 4, the experimental effect of λ with values of 0.1, 0.5, 0.7 and 0.9 respectively. In addition, Fig. 5 shows the PSNR after image restoration in Fig. 1(b) when the λ is different. In Fig. 5, the PSNR effect is the best when the correction value is about 0.7. The following parameters can also be properly corrected for the restoration of different images to achieve a better restoration effect.

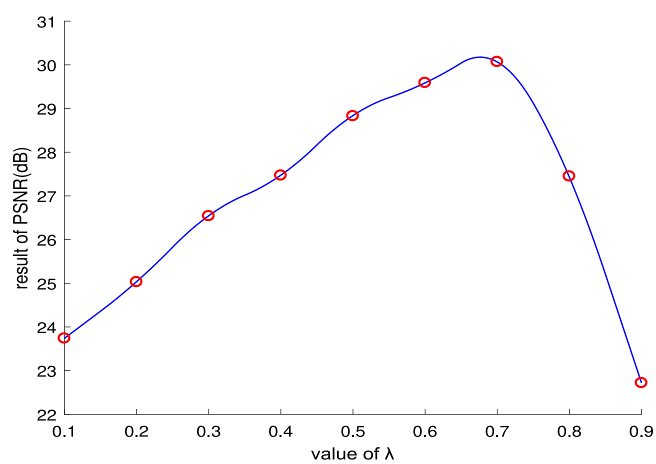

Fig. 5. PSNR of recovered images with various λ.

This paper provides a novel ringing-detecting regularization for the energy function and a texture feature map for adaptive iterations. These two approaches combine a new non-blind deconvolution algorithm that is a convincing solution to reducing the ringing of the recovered image in a single image deblurring. The pseudo code of image deconvolution using ringing-detecting regularization and a segmentation-based texture map is in Algorithm 1.

4. Experimental and discussion

Fig. 6 shows the results deblurred by two different kernels. The two kernels are approximated by Fergus et al. [14] and Krishnan et al. [16]. The results by the standard RL and TRL algorithm for comparison are presented in this paper. For the standard RL, twenty iterations for all blurry examples are performed. Figs. 6(b) and 6(c) are the results deblurred by Fergus' kernel and Figs. 6(d) and 6(e) are the results deblurred by Krishnan's kernel. As seen from these images, for the kernel estimated by Fergus' method, the standard RL shows severe ringing artifacts, but TRL algorithm result has high performance for both ringing removal and detail enhancement. For the kernel estimated by Krishnan's method, it is shown that the standard RL is adequate to reconstruct the deblurred image, and TRL algorithm result has the same sharp edges as the standard RL's while having fewer artifacts (as shown in the green rectangle in the figure). This comparison of two sets of results indicates that TRL has good robustness against ringing even if the kernel is not sufficiently accurate and avoids

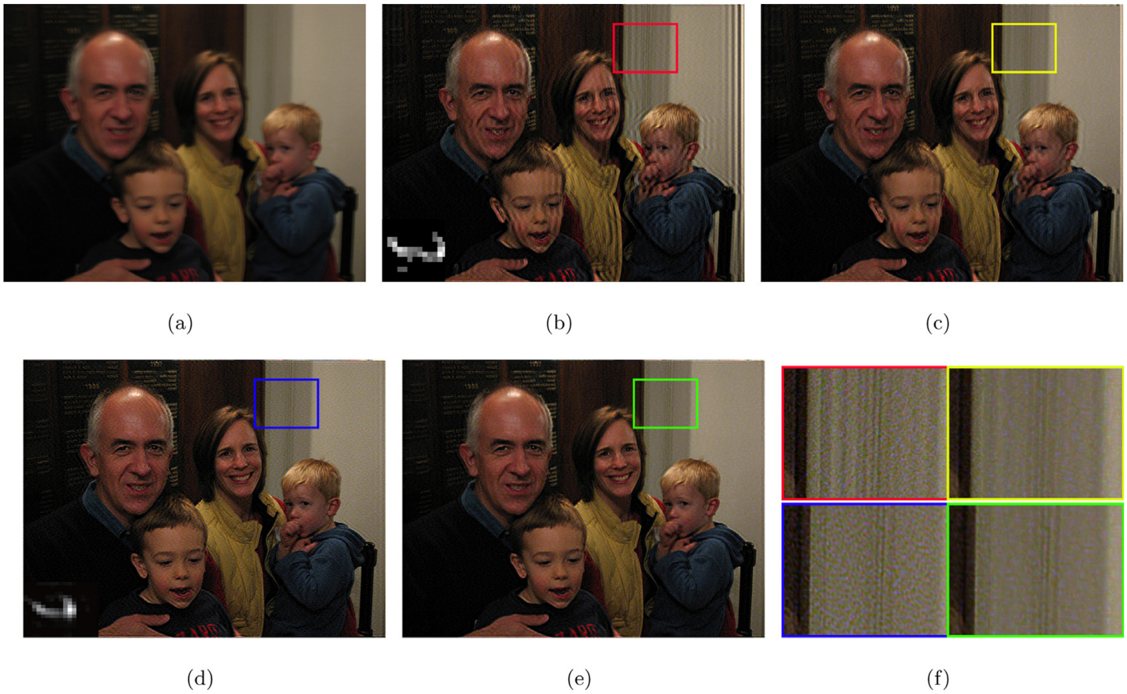

Fig. 6. Deblurred results with two different kernels. (a) The input blurry image (b) Standard RL result and PSF (lower left corner) estimated by Fergus et al. [14]. (c) Our result using PSF estimated by Fergus et al. [14]. (d) Standard RL result and the PSF (lower left corner) estimated by Krishnan et al. [16]. (e) Our result using the PSF estimated by Krishnan et al. [16]. (f) Close-up views of (b), (c), (d) and (e) correspond to the rectangles of the same color. (For interpretation of the references to color in this figure legend, the reader is referred to the web version of this article.)

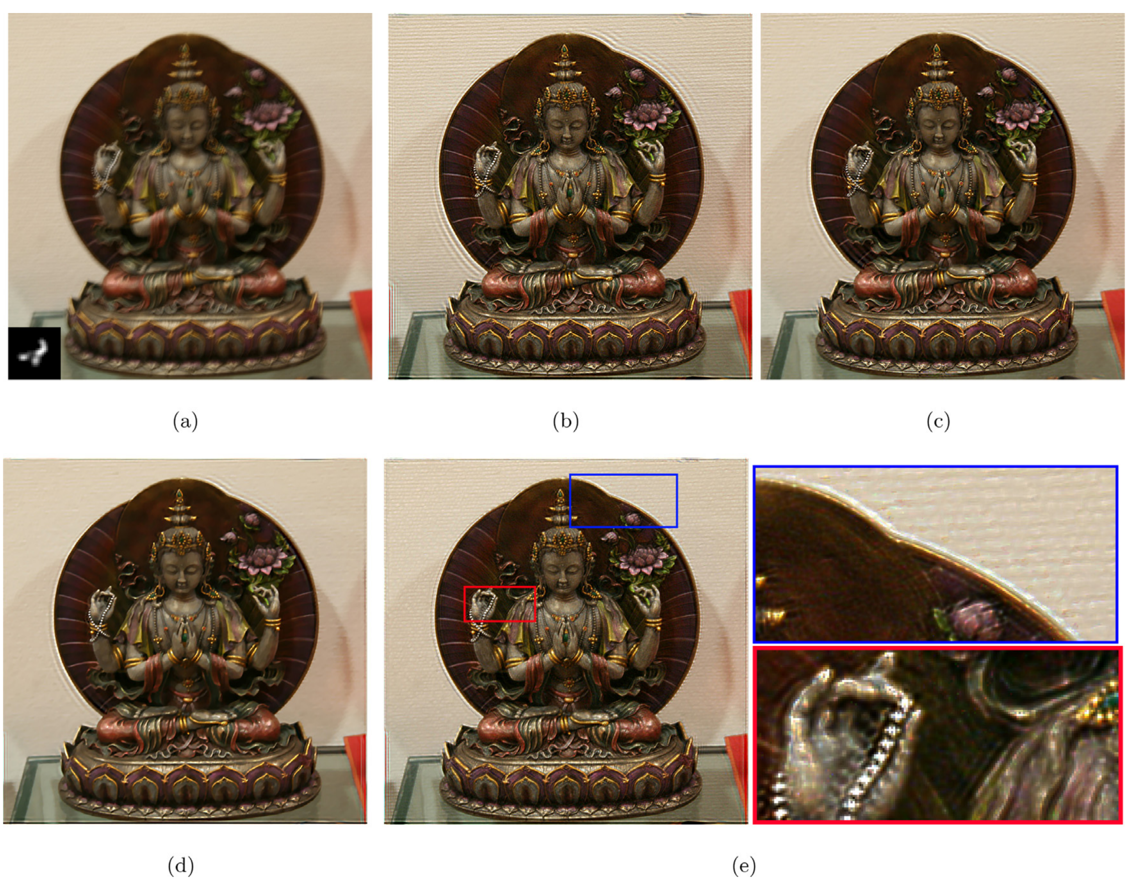

Fig. 7. (a) The input blurry image and its PSF estimated by Shan et al. [15]. (b) The standard RL result. (c) The result of Shan et al. [15]. (d) The result of TV regularization of Chan et al. [6]. (e) TRL's result and some close-ups.

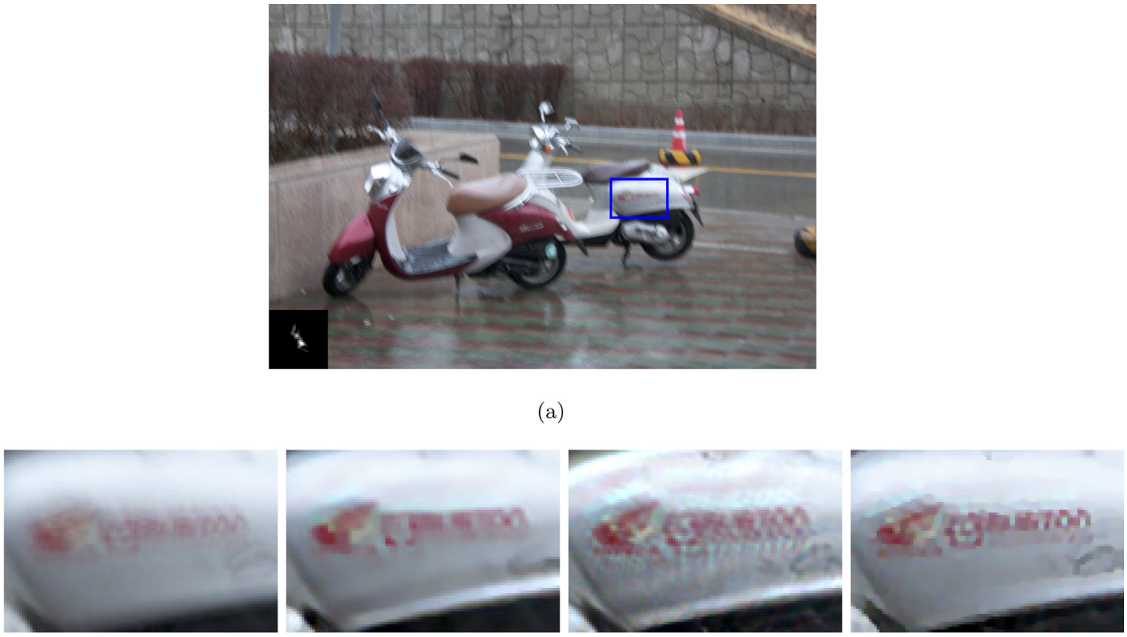

Fig. 8. Comparison to Cho et al. [19] and Yuan et al. [18]. (a) Blurred image and PSF estimated by Cho et al. [19]. (b) Blurred image. (c) The result of Cho et al. [19]. (d) The result of Whyte et al. [18]. (e) TRL's result.

Fig. 9. Comparison to Cho et al. [19] and Yuan et al. [18]. (a) Blurred image and PSF estimated by Cho et al. [19]. (b) Blurred image. (c) The result of Cho et al. [19]. (d) The result of Whyte et al. [18]. (e) TRL's result.

Fig. 10. Comparison to Pan et al. [21] and Zhang et al. [26]. (a) The blurry image and its PSF estimated by Pan et al. [21]. (b) The result of Pan et al. [21]. (c) The result of Zhang et al. [26]. (d) TRL's result.

generating over-smoothened structures in the texture region and over-sharpened details in the flat region.

To evaluate the performance of the ringing suppression and segmentation scheme on deblurring, TRL is applied on a variety of real images. In experiments, the factor λ of the TRL can be adaptively regulated. The regularization factor controls the constraint on ringing and makes a better compromise between ringing suppression and edge sharpness. For all examples, the default value of λ is set to 0.7.

In Fig. 7, TRL algorithm is compared with three superior methods of standard RL, TV regularization [6], and Shan's method [15]. The blur kernel is estimated by Shan's method. For TV

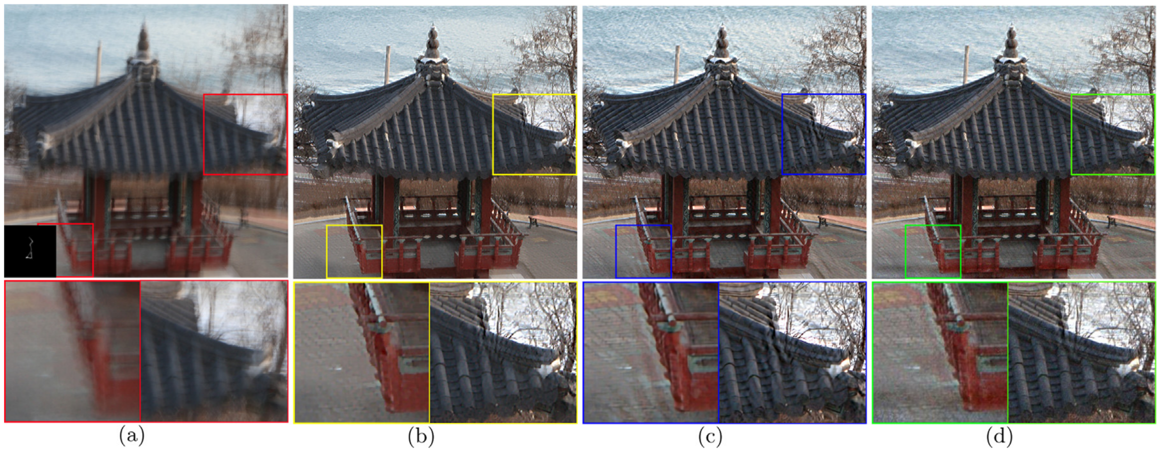

Fig. 11. Comparison to Pan et al. [21] and Zhang et al. [26]. (a) The blurry image and its PSF estimated by Pan et al. [21]. (b) The result of Pan et al. [21]. (c) The result of Zhang et al. [26]. (d) TRL's result.

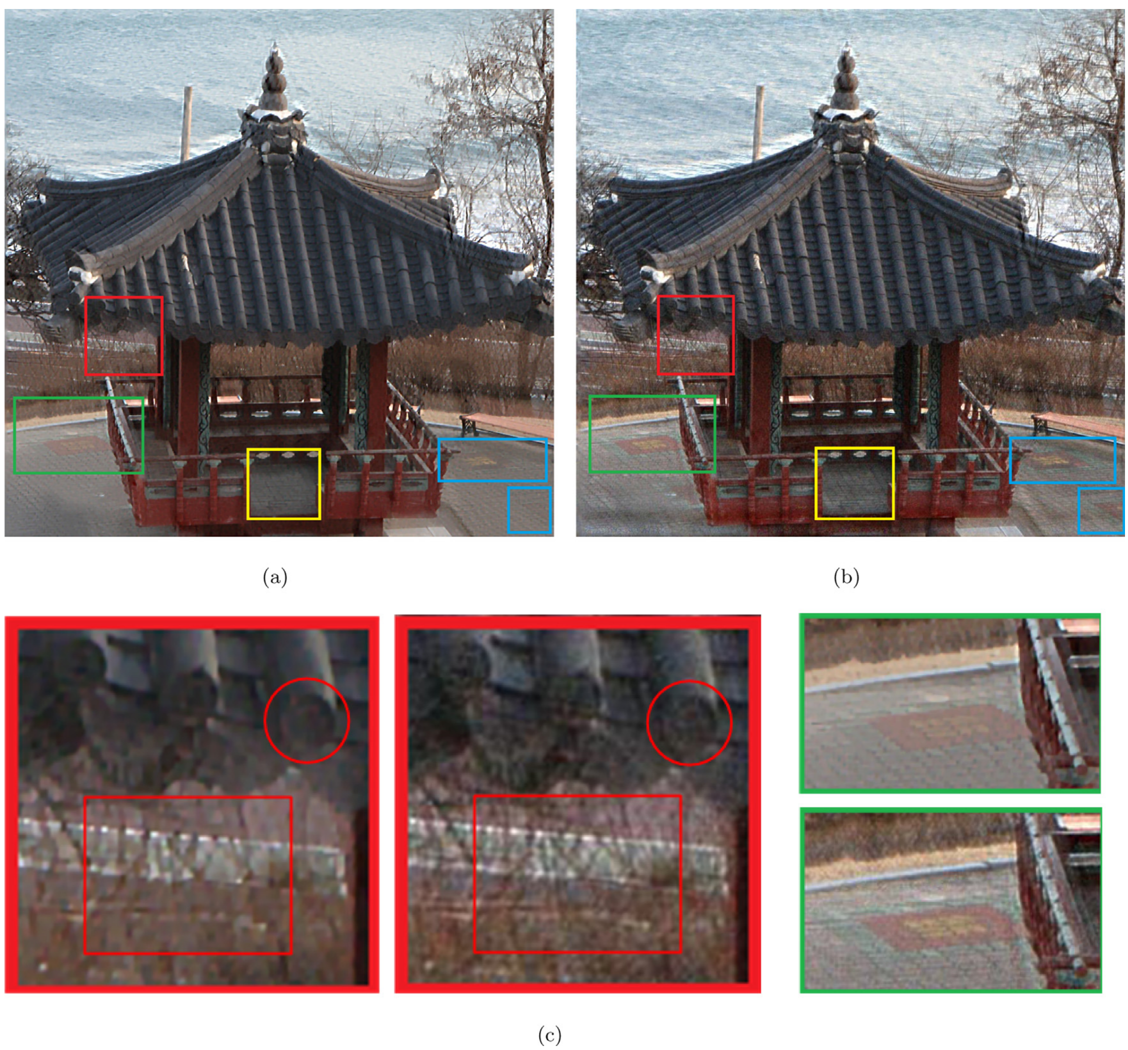

Fig. 12. Comparison to Pan et al. [21] and TRL again. (a) The result of Pan et al. [21]. (b) TRL's result. (c) The detail of the results. The right image of the red box and the bottom image of the green box are TRL's results. (For interpretation of the references to color in this figure legend, the reader is referred to the web version of this article.)

regularization, the most visually pleasing result that balances the recovered details and ringing reduction is generated by altering its regularization factors. The deblurred image produced by the standard RL has the most obvious ringing. In addition, the other two approaches can suppress the ringing artifacts to some extent but also blur or smooth details of the image. Our approach can not only recover additional image details and sharper image edges but also effectively lessen ringing.

(a) (b) (c) (d)

Fig. 13. Monkey D. Luffy taken by a Canon camera. (a) Blurred image and kernel (lower left corner) estimated by Krishnan et al. [16]. (b) The result of the standard RL. (c) Krishnan et al.'s result. (d) TRL's result.

Figs. 8 and 9 compare non-blind deblurring results. Compared to the results of Cho et al. [19], the results of the proposed method contain plainer characters and sharper edges. Based on the Richardson–Lucy algorithm, TRL algorithm generates a clearer result on a natural image and a comparable result on saturated image with Whyte et al. [18], which is specially designed for the saturated images.

Figs. 10 and 11 show examples with large blur kernels and deblurred results from the state-of-the-art methods [21,26]. For fair comparisons, the kernel estimated is used by the method [21] to generate the latent images in all algorithms. Due to the proposed adaptive iteration mechanism, TRL's result does not have significant ringing overall and preserves more salient edges and details in the restored images.

At the same time, we also further compared the details of the restoration effect of the Pan's [21] algorithm and the TRL algorithm as shown in Fig. 12. It can be seen from the detailed picture that the restoration effect of Pan's algorithm is relatively vague, and its details are not clear enough, including grass, floor tiles, railings, eaves, etc. For example, in Pan's result, the light green floor tiles in the outer ring of floor tiles have been clearly displayed, and the texture lines at the joints of the floor tiles are also blurred or even disappeared; the eaves are relatively blurred and flat, and the texture cannot be clearly restored; the texture of the grass is not clear enough. In our algorithm, the light green part of the outer circle of the floor tiles is very clear, and the detailed texture is richer; the pattern on the eaves circle is also more obvious; the grass texture is more realistic. Because our algorithm utilizes image texture, the restoration effect is better for areas with rich image texture details. This is also the reason why the quantitative indicators such as PSNR of the Pan's algorithm are relatively low. Their algorithm flattens the image too much, which will blur the details of the image.

TRL is also applied to a real image taken by a handheld camera. Fig. 13(a) is the blurry image and the estimated kernel by Krishnan et al. [16]. For the comparison, the result of the standard RL and the method of Krishnan et al. [16] is displayed. As Fig. 13 indicates, the proposed approach significantly diminishes the ringing artifacts in the deblurred image. In summary, the experimental results show that TRL algorithm brings about significantly fewer ringing artifacts.

To further illustrate the effectiveness of the proposed algorithm, information entropy of restored images is calculated. Information entropy reflects the average amount of information conveyed by each pixel in the image, which can measure the importance of the target in the image. The greater the information entropy, the more information is contained in the image. Table 1 shows information entropy of recovered images of different algorithms in Figs. 6 to 13, and the bold fonts indicates the optimal value of each set of results. It can be seen from Table 1 that TRL's results have a higher information entropy, which indicates that this method can recover more details from the blurred image.

Table 1
Information entropy of recovered images in Figs. 4 to 10.

Image	Fig. 6	Fig. 7	Fig. 8	Fig. 9	Fig. 10	Fig. 11	Fig. 12
Sub-graph (a)	6.8811	7.6648	–	–	7.0058	7.5275	6.7912
Sub-graph (b)	6.8231	7.7549	7.5750	7.4574	7.0357	7.6728	**6.9658**
Sub-graph (c)	**6.8924**	7.6993	7.5622	7.4477	7.0010	7.7558	6.8801
Sub-graph (d)	6.8112	7.6909	7.5770	7.5877	**7.1367**	**7.7611**	6.8870
Sub-graph (e)	6.8853	**7.7745**	**7.5935**	**7.6245**	–	–	–

Table 2
PSNR, SSIM and inference efficiency of different algorithms.

	PSNR	SSIM	Runtime
Cho et al. [19]	26.32	0.862	2.4
Yuan et al. [18]	27.03	0.869	3.5
Pan et al. [21]	27.82	0.897	5.7
Zhang et al. [26]	27.38	0.876	8.3
DeblurGAN-v2 [35]	29.89	0.907	9.1
MPRNet [36]	30.24	0.916	17.4
MIMO-UNet [34]	31.08	0.918	7.8
TRL	31.73	0.925	3.2

Due to the recent success of Convolutional Neural Networks (CNN) and Generative Adversarial Networks (GAN) in object detection [22], recognition [23] and related tasks [24], some scholars have tried to use deep learning for motion blur images recovery. TRL is also compared with a popular deep learning algorithm MIMO-UNet [34], as shown in Fig. 14. TRL is based on a single image for restoration, and MIMO-UNet needs to use a data set for training, the result in Fig. 14 is obtained by using the training weight provided by the authors [34]. Since the MIMO-UNet model has requirements for the size of the input image, the results are compared after cropping the pictures used in the previous part. In Fig. 14, we can see that the effect of MIMO-UNet is not very satisfactory. This is also a common problem of current deep learning algorithms. It requires a lot of training to get better results. However, there is often only one single image instead of large data set for training in the actual restoration work. This is also the advantage of TRL algorithm.

At the same time, we use the training data set GoPro which was also used by MIMO-UNet [34] for testing. In Fig. 15, our algorithm is not as effective as MIMO-UNet. Our algorithm is based on the restoration of a single picture, while MIMO-UNet is a deep learning training conducted on this data set GoPro. Therefore, our result is also acceptable practically.

In order to quantify the superiority of TRL algorithm, standard performance indicators (PSNR, SSIM) and inference efficiency (average running time per image measured are compared on an

(a) (b) (c)

Fig. 14. Deblurred results with MIMO-UNet [34] and TRL using the images mentioned above. (a) The input blurry images. (b) The results of MIMO-UNet [34]. (c) The results of TRL.

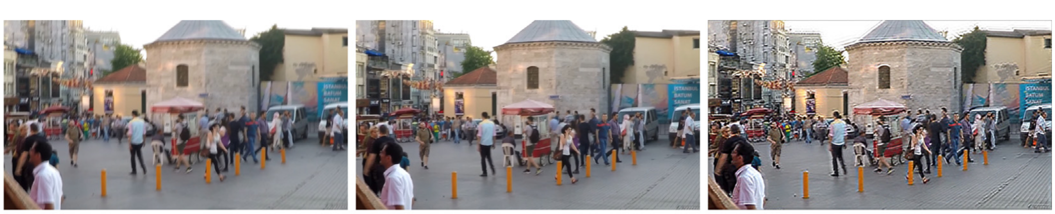

(a) (b) (c)

Fig. 15. The results of the image deblurred result of the GoPro dataset used by the MIMO-UNet model and TRL. (a) The input blurry image. (b) The result of MIMO-UNet. (c) The result of TRL.

(a) (b)

Fig. 16. More results of TRL, including the dataset of [21] (temple eaves and license plate) and photograph taken by the author (author's pet cat). (a) The input blurry images. (b) The results of TRL.

8-core CPU) are carried out using more than 800 images. The images size resize to 1 million pixels. The running time is expressed in seconds. TRL is compared with many state-of-the-art methods, among whom are not only traditional algorithms, but also deep learning algorithms. It can be seen from Table 2 that in terms of average PSNR and SSIM, TRL is higher than other algorithms and run much faster than deep learning algorithms. Meanwhile, TRL has 50% less inference time than MIMO-UNet. The reason may be that deep learning is slow to run in CPU environment.

Moreover, we also added more representative pictures (temple eaves and license plate) in the dataset of [21] and pictures taken by mobile phone in the life (author's pet cat) to show the effect of the TRL algorithm. It can be seen from Fig. 16 that the recovery effect of the TRL algorithm is very good.

The TRL algorithm not only has a remarkable restored effect but also is convenient and efficient. Compared with the popular deep learning motion blur image restoration algorithm in recent years, the TRL algorithm does not need to train a large number of data set in advance, achieving directly restored results by providing the target image. While the deep learning algorithm often needs a large number of data sets for training in one scene for image restoration, retraining is required for another scene.

5. Conclusion

A new method named TRL is applied to suppress disturbing ringing artifacts during image deconvolution while ensuring better restoration. TRL uses regularization to suppress ringing by quantifying ringing through a pyramid of multi-scale image pairs with low-pass filters of two sizes. Besides, TRL calculates the image texture using a Gaussian mixture model. The image is classified according to the flatness and similarity of the texture map, and performs different iterations in different areas to achieve a better reconstruction effect of the image and suppress the ringing. Experimental results show that the combination of regularization and adaptive segmentation-based iteration can fully balance the ringing suppression and edge restoration in deblurred images. In conclusion, our method is superior to other methods in terms of speed and accuracy. In future work, the image texture map will further be optimized to achieve a better restoration effect.

Declaration of competing interest

The authors declare that they have no known competing financial interests or personal relationships that could have appeared to influence the work reported in this paper.

Acknowledgments

This work is supported by the Beijing Municipal Science and Technology Project under the grant number (Z191100001419009).

References

[1] Helstrom CW. Image restoration by the method of least squares. JOSA 1967;57(3):297–303.
[2] Hunt BR. The application of constrained least squares estimation to image restoration by digital computer. IEEE Trans Comput 1973;100(9):805–12.
[3] Richardson WH. Bayesian-based iterative method of image restoration. JOSA 1972;62(1):55–9.
[4] Lucy LB. An iterative technique for the rectification of observed distributions. Astron J 1974;79:745.
[5] Chan TF, Wong C-K. Total variation blind deconvolution. IEEE Trans Image Process 1998;7(3):370–5.
[6] Chan SH, Khoshabeh R, Gibson KB, Gill PE, Nguyen TQ. An augmented Lagrangian method for total variation video restoration. IEEE Trans Image Process 2011;20(11):3097–111.
[7] Xiang J, Ye P, Wang L, He M. A novel image-restoration method based on high-order total variation regularization term. Electronics 2019;8(8):867.
[8] Levin A, Fergus R, Durand F, Freeman WT. Image and depth from a conventional camera with a coded aperture. ACM Trans Graph 2007;26(3):70–es.
[9] Yi B, Manchester IR. On the equivalence of contraction and koopman approaches for nonlinear stability and control. 2021, arXiv preprint arXiv:2103.15033.
[10] Liu Y, Wang J, Cho S, Finkelstein A, Rusinkiewicz S. A no-reference metric for evaluating the quality of motion deblurring. ACM Trans Graph 2013;32(6):1–12.
[11] Wang Q, Tan J, Xing T, Chen F, Niu J. SID: Sensor-assisted image deblurring system for mobile devices. IEEE Access 2019;7:146607–19.
[12] Yang C, Feng H, Xu Z, Chen Y, Li Q. Image deblurring utilizing inertial sensors and a short-long-short exposure strategy. IEEE Trans Image Process 2020;29:4614–26.
[13] Mosleh A, Green P, Onzon E, Begin I, Pierre Langlois J. Camera intrinsic blur kernel estimation: A reliable framework. In: Proceedings of the IEEE conference on computer vision and pattern recognition. 2015, p. 4961–8.
[14] Fergus R, Singh B, Hertzmann A, Roweis ST, Freeman WT. Removing camera shake from a single photograph. In: ACM SIGGRAPH 2006 papers. 2006, p. 787–94.
[15] Shan Q, Jia J, Agarwala A. High-quality motion deblurring from a single image. Acm Trans Graph (Tog) 2008;27(3):1–10.
[16] Krishnan D, Tay T, Fergus R. Blind deconvolution using a normalized sparsity measure. In: CVPR 2011. IEEE; 2011, p. 233–40.
[17] Banham MR, Katsaggelos AK. Digital image restoration. IEEE Signal Process Mag 1997;14(2):24–41.
[18] Whyte O, Sivic J, Zisserman A. Deblurring shaken and partially saturated images. Int J Comput Vis 2014;110(2):185–201.
[19] Cho S, Wang J, Lee S. Handling outliers in non-blind image deconvolution. In: 2011 international conference on computer vision. IEEE; 2011, p. 495–502.
[20] Yang L, Ji H. A variational EM framework with adaptive edge selection for blind motion deblurring. In: The IEEE conference on computer vision and pattern recognition (CVPR). 2019.
[21] Pan J, Hu Z, Su Z, Yang M-H. *l*_0-Regularized intensity and gradient prior for deblurring text images and beyond. IEEE Trans Pattern Anal Mach Intell 2016;39(2):342–55.
[22] Mohamed A, Qian K, Elhoseiny M, Claudel C. Social-STGCNN: A social spatio-temporal graph convolutional neural network for human trajectory prediction. 2020, arXiv preprint arXiv:2002.11927.
[23] Wang K, Peng X, Yang J, Meng D, Qiao Y. Region attention networks for pose and occlusion robust facial expression recognition. IEEE Trans Image Process 2020;29:4057–69.
[24] Wang S-Y, Wang O, Zhang R, Owens A, Efros AA. CNN-generated images are surprisingly easy to spot... for now. 2019, arXiv preprint arXiv:1912.11035.
[25] Li Y, Tofighi M, Geng J, Monga V, Eldar YC. Efficient and interpretable deep blind image deblurring via algorithm unrolling. IEEE Trans Comput Imaging 2020;6:666–81.
[26] Zhang K, Zuo W, Gu S, Zhang L. Learning deep CNN denoiser prior for image restoration. In: Proceedings of the IEEE conference on computer vision and pattern recognition. 2017, p. 3929–38.
[27] Li L, Pan J, Lai W-S, Gao C, Sang N, Yang M-H. Learning a discriminative prior for blind image deblurring. In: Proceedings of the IEEE conference on computer vision and pattern recognition. 2018, p. 6616–25.
[28] Shen Z, Wang W, Shen J, Ling H, Xu T, Shao L. Human-aware motion deblurring. In: IEEE international conference on computer vision. 2019.
[29] Lu B, Chen J-C, Chellappa R. Unsupervised domain-specific deblurring via disentangled representations. In: Proceedings of the IEEE conference on computer vision and pattern recognition. 2019, p. 10225–34.
[30] Kaufman A, Fattal R. Deblurring using analysis-synthesis networks pair. 2020, arXiv preprint arXiv:2004.02956.
[31] Holoborodko P. Noise robust gradient operators. 2009, http://www.holoborodko.com/pavel/image-processing/edge-detection/.
[32] Teo P, Heeger D. Perceptual image distortion. In: Proceedings of 1st international conference on image processing, Vol. 2. 1994, p. 982–6.
[33] Wang Z, Bovik A, Sheikh H, Simoncelli E. Image quality assessment: from error visibility to structural similarity. IEEE Trans Image Process 2004;13(4):600–12.
[34] Cho S-J, Ji S-W, Hong J-P, Jung S-W, Ko S-J. Rethinking coarse-to-fine approach in single image deblurring. In: Proceedings of the IEEE/CVF international conference on computer vision. 2021, p. 4641–50.
[35] Kupyn O, Martyniuk T, Wu J, Wang Z. DeblurGAN-v2: Deblurring (orders-of-magnitude) faster and better. In: 2019 IEEE/CVF international conference on computer vision (ICCV). 2019.
[36] Zamir SW, Arora A, Khan S, Hayat M, Khan FS, Yang M-H, Shao L. Multi-stage progressive image restoration. In: 2021 IEEE/CVF conference on computer vision and pattern recognition (CVPR). 2021, p. 14816–26.